Approximate bounds and temperature dependence of adiabatic connection integrands for the uniform electron gas

Brittany P. Harding,[1] Zachary Mauri,[1] and Aurora Pribram-Jones[1]
University of California, Merced, 5200 North Lake Road, Merced, CA 95343

(*Electronic mail: apj@ucmerced.edu)

(Dated: 15 February 2022)

Thermal density functional theory is commonly used in simulations of warm dense matter, a highly energetic phase characterized by substantial thermal effects and by correlated electrons demanding quantum mechanical treatment. Methods that account for temperature dependence, such as Mermin-Kohn-Sham finite-temperature density functional theory and free energy density functional theory, are now employed with more regularity and available in many standard code packages. However, approximations from zero-temperature density functional theory are still often used in temperature-dependent simulations by using thermally weighted electronic densities as input to exchange-correlation functional approximations, a practice known to miss temperature-dependent effects in the exchange-correlation free energy of these systems. In this work, the temperature-dependent adiabatic connection is demonstrated and analyzed using a well-known parameterization of the uniform electron gas free energy. Useful tools based on this formalism for analyzing and constraining approximations of the exchange-correlation at zero temperature are leveraged for the finite-temperature case. Inspired by the Lieb-Oxford inequality, which provides a lower bound for the ground-state exchange-correlation energy, bounds for the exchange-correlation at finite temperatures are approximated for various degrees of electronic correlation.

I. INTRODUCTION

Recent decades have seen a rapid growth of interest in the study of matter under conditions of extreme excitation and/or compression. This interest includes growing focus on warm dense matter (WDM), a highly energetic phase characterized by the simultaneous existence of strongly-correlated electrons, thermal effects, and quantum effects of electrons.[1–5] Astrophysical examples of WDM include white dwarf atmospheres and planetary cores,[6,7] while more down-to-earth examples include laser-excited solids and inertial confinement fusion capsules.[8–10] There have been corresponding advances in the use of density functional theory[11,12] (DFT) calculations of WDM. Aside from describing planetary interiors,[13–15] these calculations are useful for predicting material properties,[4,5,16] developing experimental standards,[3,17] and supplementing experiments that push the boundaries of accessible conditions.[18–21]

In many thermal DFT calculations, a small-but-crucial free energy component, called the exchange-correlation (XC), is approximated by a ground-state approximation. However, in principle, the XC free energy depends explicitly on temperature.[22–25] If the exact temperature-dependent XC free energy were known, the free energy and density for a given distribution of the nuclei, and any properties that could be extracted from these, such as Hugoniot shock curves and equations of state of materials, could be predicted exactly.[26] While using a ground-state approximation to the XC free energy has not been shown to be a fatal flaw, its shortcomings continue to be investigated via comparison with existing temperature-dependent XC approximations and through analysis of model systems.[4,5,21,27–37]

Approximations to the XC functional can be informed by the adiabatic connection formalism (ACF), which is an important analytical and interpretive tool in DFT.[38–40] The ACF expresses $E_{\mathrm{XC}}[n]$ exactly as an integral over the coupling constant, λ, which smoothly connects the fictitious non-interacting Kohn-Sham reference system ($\lambda = 0$) with the real physical interacting system ($\lambda = 1$), while holding the density fixed. A similar theoretical construction with explicit temperature dependence for an ensemble at finite temperature exists,[25] but it has only been numerically demonstrated as it has for zero-temperature systems using model systems such as the Hubbard dimer.[30,41]

A useful tool in the quest for better functional approximations is the list of known exact properties and constraints on the formally exact XC functional.[42,43] The Lieb-Oxford (LO) bound[44–51] is an exact inequality that provides a strict bound on the XC energy, and it has been used to constrain some of the most successful XC approximations. Perdew derived looser lower bounds on the XC and exchange energies using the LO lower bound on the indirect Coulomb energy,[52] which was subsequently used in the development of the Perdew-Burke-Ernzerhof approximation.[53] While GGAs must violate this constraint for realistic energetic predictions,[54] a meta-GGA that satisfies important constraints, including the LO bound, was constructed by Sun and collaborators.[55] The few temperature-dependent XC approximations developed in the literature[56] are constructed to satisfy the LO bound, but the effect of temperature on this formal relationship has not been explored in a detailed manner.

In this work, finite-temperature adiabatic connection (FT AC) curves are generated using a parameterization[57] of the XC free energy of the uniform electron gas (UEG) for various temperatures and densities in the WDM regime. In order to validate the finite-temperature simulated scaling approach used in this work, calculated XC free energy values are compared to XC free energy values generated from the Fortran 90 program provided by Groth and collaborators,[57] upon which the simulated scaling results also rely. In addition, the behavior of simulated curves is evaluated in light of known mathematical conditions on the exchange free energy. The calculated adiabatic connection curves are used to explore how the balance between exchange and correlation changes in different regimes. Subsequently, adherence to the LO bound is analyzed and an approach to estimating temperature-dependence is evaluated. Approximate bounds are generated numerically using these results and compared to those known at zero-temperature (ZT).

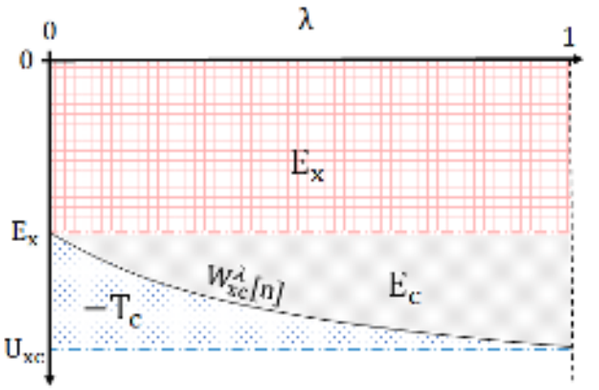

FIG. 1. A diagram of the adiabatic connection at zero temperature. The area in red, E_{X}, represents the exchange energy component of E_{XC}, while the gray area, E_{C}, depicts the correlation energy component. The blue shaded region is related to the kinetic correlation component of E_{XC}.

II. BACKGROUND

Hohenberg and Kohn have shown[11] that there exists a functional of the density such that

$$E \equiv \int d\mathbf{r}\, v(\mathbf{r}) n(\mathbf{r}) + F[n(\mathbf{r})] \tag{1}$$

is equal to the ground-state energy when $n(\mathbf{r})$ is the ground-state density.[11] DFT relies on the fact that the ground-state energy is expressed as a functional of the ground-state density. The core idea of Kohn-Sham DFT,[12] one of the most successful approaches to the many-body problem, is to approach the interacting problem of interest by mapping it to a more tractable non-interacting problem. This mapping would be exact if the correct exchange-correlation (XC) functional for arbitrary physical systems was available. However, this is not the case in the vast majority of systems, and so one must use approximations for practical calculations.

The ZT adiabatic connection gives an exact expression for the exchange-correlation functional,

$$E_{\mathrm{XC}}[n] = \int_0^1 d\lambda W_{\mathrm{XC}}^{\lambda}[n], \tag{2}$$

expressed as an integral over a coupling constant λ, which, while holding the density $n(\mathbf{r})$ fixed, continuously connects the KS reference system ($\lambda = 0$) with the real, physical interacting system ($\lambda = 1$).[38–40] The integrand, $W_{\mathrm{XC}}^{\lambda}[n]$, is generated by introducing λ into the universal functional, $F^{\lambda}[n] = \min_{\Psi\to n}\langle\Psi|\hat{T} + \lambda\hat{V}_{ee}|\Psi\rangle$, where Ψ is the minimizing wave function for a given λ. For all values of λ, the density remains that of the real physical system (the superscript λ is often omitted when $\lambda = 1$). An illustration of the adiabatic connection, which provides a geometrical representation of the components of E_{XC}, is shown in Fig. 1.

Moving to non-zero temperatures requires shifting our focus from ground-state energy functionals to free energy functionals. Mermin[22] generalized the Hohenberg-Kohn (HK) theorems to equilibrium systems at finite temperatures. At non-zero temperatures, many-electron systems can be described by the grand-canonical ensemble. The grand potential[25] can be written,

$$\hat{\Omega} = \hat{H} - \tau\hat{S} - \mu\hat{N}, \tag{3}$$

where $\hat{H}$ represents the electronic Hamiltonian operator, τ the temperature, $\hat{S}$ the entropy operator, μ the chemical potential, and $\hat{N}$ the particle-number operator. The entropy operator is defined via,

$$\hat{S} = -k_B \ln\hat{\Gamma}, \tag{4}$$

where $\hat{\Gamma}$ is the statistical operator,

$$\hat{\Gamma} = \sum_{N,i} w_{\mathrm{N,i}} |\Psi_{\mathrm{N,i}}\rangle\langle\Psi_{\mathrm{N,i}}|. \tag{5}$$

Orthonormal N-particle states are denoted by $|\Psi_{\mathrm{N,i}}\rangle$, and the normalized statistical weights, $w_{\mathrm{N,i}}$, satisfy $\sum_{\mathrm{N,i}} w_{\mathrm{N,i}} = 1$. One obtains a set of thermal KS equations through a mapping similar to the ZT one, but this time keeping both the equilibrium density and temperature fixed. In the ZT case, we focused on the ground-state density, but here the fundamental object, generated by the equilibrium statistical operator, is the thermally weighted, equilibrium density. This mapping and energy decomposition defines the XC free energy, which now includes an entropic term. The Mermin-Kohn-Sham (MKS) equations[12,22] are similar to the ground-state KS equations, but are complicated by temperature-dependent eigenvalues, eigenstates, and effective potential. This yields the MKS den-

sity, which is equal to the exact equilibrium density by definition:

$$n^\tau(\mathbf{r}) = \sum_i f_i^\tau |\phi_i^\tau(\mathbf{r})|^2, \tag{6}$$

where $\phi_i^\tau(\mathbf{r})$ is the i^{th} eigenstate, and f_i^τ is the state's corresponding Fermi occupation. The free energy of the physical system is written in the usual way,[26]

$$A = T - \tau S + V_{ee} + V_{\text{ext}}, \tag{7}$$

where T is the kinetic energy, S is the entropy, V_{ee} is the electron-electron repulsion, and V_{ext} is the external, nuclear potential.[58] To emphasize the tied coordinate-temperature scaling relationships in thermal DFT, we can write the kentropy[25] as $K = T - \tau S$. The same equation for the free energy of the systems can be written in terms of the corresponding KS quantities:

$$A = T_s - \tau S_s + U + A_{\text{XC}} + V_{\text{ext}}, \tag{8}$$

where the subscript s denotes the KS quantities, U is the Hartree energy, and A_{xc} is the XC free energy. Mirroring the interacting case, the non-interacting kentropy is written $K_s = T_s - \tau S_s$.

While the operators of quantum mechanics scale in a simple way, the conversion to density functionals invites some complexity. One commonly exploited relationship in modern DFT is that between coordinate scaling and the coupling constant.[59] When the length scale of our system is changed by a factor γ, we can maintain the normalization of the system via the following definition of the scaled ZT density:

$$n_\gamma(\mathbf{r}) = \gamma^3 n(\gamma \mathbf{r}). \tag{9}$$

Using this scaled density as input, straightforward scaling of energy quantities result, unless the quantities include correlation.

In the adiabatic connection, a coupling constant, λ, is introduced into the universal functional,[42,59]

$$F^\lambda[n] = \min_{\Psi \to n} \langle \Psi | \hat{T} + \lambda \hat{V}_{ee} | \Psi \rangle, \tag{10}$$

where, again, $\lambda = 0$ yields the fictitious KS system and $\lambda = 1$ gives the real, interacting system of interest. For all values of λ, the density is that of the physical system. The universal functional can be combined with coordinate and density scaling relationships, yielding the relation,

$$F^\lambda[n] = \lambda^2 F[n_{1/\lambda}]. \tag{11}$$

Here, the fully interacting functional evaluated on a scaled density is multiplied by the square of the inverse of the density scaling factor, giving access to the universal functional at a scaled interaction strength. Explicitly known conditions on other energy components can be written under concurrent coordinate and interaction strength scaling, as we will see later.[39,42]

The same concepts applied in ZT simulated interaction strength scaling can be extended to the finite-temperature adiabatic connection (FTAC),[25,60]

$$A_{\text{XC}}^\tau[n] = \int_0^1 d\lambda W_{\text{XC}}^{\tau,\lambda}[n], \tag{12}$$

where here, the adiabatic connection integrand is both temperature- and interaction strength–dependent: $W_{\text{XC}}^{\tau,\lambda}[n] = U_{\text{XC}}^{\tau,\lambda}[n]/\lambda$. The extension of Eqn. 11 to finite temperature is written as $F^{\tau,\lambda}[n] = \lambda^2 F^{\tau/\lambda^2}[n_{1/\lambda}]$. Throughout this work, we follow standard practice: the temperature at which a functional is evaluated appears as a superscript, subscripts refer to coordinate scaling, and superscripts indicate interaction strength scaling. Lack of a λ superscript implies that $\lambda = 1$. An illustration of the adiabatic connection generalized to finite temperatures is shown in Fig. 2. The red arrow indicates the monotonic behavior of the exchange free energy component, $A_{\text{X}}[n]$, which increases with increasing temperature. On the other hand, the correlation free energy component, A_{C}, shows more complex behavior, and varies non-monotonically as the temperature increases.

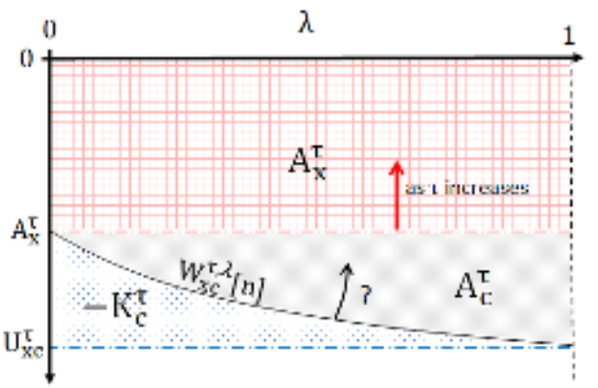

FIG. 2. A diagram of the finite-temperature adiabatic connection. The area in red depicts the exchange free energy component of A_{XC}, the gray area represents the correlation free energy, and K_{C} is the kentropic correlation (the FT analog of the kinetic correlation). While the behavior of A_{X} for a fixed r_s with increasing temperature is predictable, the temperature-dependent behavior of A_{C} is more complex.

III. METHODS

When discussing the uniform gas, constraints on the density functions describing the system are similar to those on density functionals[42] and can be used to extract useful information about properties such as limiting behavior. For instance, coor-

TABLE I. Comparison of the XC free energy per particle values generated using the Fortran 90 program[57] provided by Groth and collaborators and values obtained via integration of simulated scaling curves (FTAC) at three different temperatures and values of the Wigner-Seitz radius. Improved agreement with the Fortran values (reported in Hartree) can be obtained by increasing the resolution in interaction strength, λ, in the numerical implementation of simulated scaling.

	$r_s = 1$		$r_s = 2$		$r_s = 4$	
	Groth *et al.*	**FT AC**	**Groth *et al.***	**FT AC**	**Groth *et al.***	**FT AC**
$\tau = 0.1$	-0.51668	-0.51667	-0.27194	-0.27192	-0.13375	-0.13374
$\tau = 0.5$	-0.50031	-0.50027	-0.22335	-0.22335	-0.08779	-0.08779
$\tau = 1.0$	-0.45919	-0.45922	-0.18167	-0.18167	-0.06731	-0.06731

dinate scaling can be expressed in terms of interaction strength scaling in the expression for the XC free energy per particle:

$$a_{\mathrm{XC}}^{\tau,\lambda}(n) = \lambda^2 a_{\mathrm{XC}}^{\tau/\lambda^2}\left(n_{1/\lambda}\right). \tag{13}$$

The exchange free energy per particle, now expressed in terms of the Wigner-Seitz radius, r_s, can be extracted by scaling to the high-density limit of the FT uniform gas:[53,61,62]

$$a_{\mathrm{X}}^{\tau}(r_s) = \lim_{\gamma\to\infty} \frac{a_{\mathrm{XC}}^{\gamma^2\tau}\left(\frac{r_s}{\gamma}\right)}{\gamma}. \tag{14}$$

The expression for the correlation component of the free energy per particle is then obtained using the simple relationship between exchange and correlation:

$$a_{\mathrm{C}}^{\tau}(r_s) = a_{\mathrm{XC}}^{\tau}(r_s) - a_{\mathrm{X}}^{\tau}(r_s). \tag{15}$$

These results of tied coordinate–temperature–interaction strength scaling can be combined to extract any component of the correlation free energy from any other piece.[60] We extract the potential contribution from the full correlation free energy per particle via,

$$u_{\mathrm{C}}^{\tau}\left(\frac{r_s}{\gamma}\right) = -\gamma\frac{da_{\mathrm{C}}^{\gamma^2\tau}\left(\frac{r_s}{\gamma}\right)}{d\gamma} + 2a_{\mathrm{C}}^{\gamma^2\tau}\left(\frac{r_s}{\gamma}\right), \tag{16}$$

and combine it with the definition of the FT adiabatic connection integrand for the uniform gas,

$$W_{\mathrm{C}}^{\tau,\lambda}(r_s) = \frac{u_{\mathrm{C}}^{\tau,\lambda}(1/r_s)}{\lambda} = \frac{\lambda^2 u_{\mathrm{C}}^{\tau/\lambda^2}(\lambda r_s)}{\lambda} = \lambda u_{\mathrm{C}}^{\tau/\lambda^2}(\lambda r_s). \tag{17}$$

This yields the finite-temperature adiabatic connection integrand in terms of $a_{\mathrm{C}}^{\tau}(r_s)$ evaluated at carefully scaled densities and temperatures. This process is usually used for generation of ACF curves at zero-temperature and is called simulated scaling.[63,64] The final expression for $W_{XC}^{\tau,\lambda}$ is the sum of $W_{C}^{\tau,\lambda}$ and the λ-independent, FT exchange component from Eq. 14:

$$W_{\mathrm{XC}}^{\tau,\lambda}(r_s) = \lambda u_{\mathrm{C}}^{\tau/\lambda^2}(\lambda r_s) + \lim_{\gamma\to\infty}\frac{a_{\mathrm{xc}}^{\gamma^2\tau}(r_s/\gamma)}{\gamma}. \tag{18}$$

This ACF allows us to calculate the temperature-dependent correlation free energy per particle at any coupling constant strength and temperature. To do so, we use the parametrization in Ref. 57 for the FT UEG and construct FTAC curves at varying density and temperature conditions, using Mathematica Version 11.2.[65] Table 1 compares values of the XC free energy per particle, obtained from the Fortran 90 code provided by Groth and collaborators, to values obtained using the FTAC formalism. The agreement between the values obtained from the formalism in this work and the Fortran code, and its controllable accuracy via increased interaction strength resolution, verifies the validity of the implemented simulated scaling technique.

Another verification that our application of simulated scaling is sound relies on known behavior of the exchange free energy for the uniform gas. The XC free energy in this work is expressed as a function of the electron degeneracy parameter or reduced temperature,

$$\theta = \frac{2\tau}{(3\pi^2 n)^{2/3}} = 2\tau r_s^2\left(\frac{4}{9\pi}\right)^{2/3}. \tag{19}$$

The ground-state exchange can be related to a_{X}^{τ} via a thermal reduction factor, R_{X}, where R_{X} can only depend on temperature and density through θ, the electron degeneracy parameter:[24,26]

$$a_{\mathrm{X}}^{\tau}(r_s) = \varepsilon_{\mathrm{X}}^{\mathrm{unif}}(r_s) R_{\mathrm{X}}(\theta). \tag{20}$$

The thermal reduction factor decreases with increasing θ, meaning that as the electron degeneracy increases, the exchange free energy per particle decreases in magnitude.

To further validate the use of simulated scaling at finite temperatures, FTAC curves were generated with the same θ value. These should have the same ratio $W_{\mathrm{XC}}^{\tau,\lambda}/\varepsilon_{\mathrm{X}}^{\mathrm{unif}}$ at $\lambda = 0$. Since θ is a function of τ and r_s, individual characteristics can be scaled while the electron degeneracy remains constant. Dividing W_{XC} by the exact ground-state exchange demonstrates this equivalency. If the electron degeneracy is constant for a set of curves, then the ratio $a_{\mathrm{X}}^{\tau}/\varepsilon_{\mathrm{X}}^{\mathrm{unif}}$ should also be equivalent for all three curves. As the exchange is constant over interaction strength, plotting the FTAC in this manner exposes the correlation component of the XC free energy for pairs of r_s and τ that yield the same electron degeneracy. Fig. 3 shows sets of curves for three different electron degeneracy values,

both at low interaction strengths and up to $\lambda = 1$, the physical interaction strength. These are plotted against a logarithmic scale in λ, to demonstrate the expected behavior at $\lambda = 0$. The complicated dependence of correlation on the electron degeneracy arises at relatively low interaction strength, with the set of curves having three times the reference degeneracy crossing those of the $2\theta_0$ set almost immediately, before even a tenth of the physical interaction strength is reached.

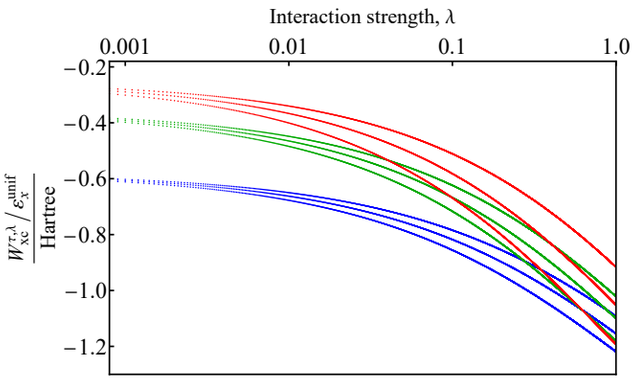

FIG. 3. $W_{xc}^{\tau,\lambda}(r_s)/\varepsilon_x^{unif}(r_s)$ is plotted against a logarithmic scale in λ for an arbitrary reference electron degeneracy, θ_0, using combinations of r_s and τ to produce three curves with equivalent electron degeneracies (Eq. 18). At low interaction strength, λ, all three curves in a set with the same electron degeneracy meet at the y-axis. Curves plotted for two additional values of θ, which are simply scaled values of θ_0, demonstrate the same behavior and further validate the use of simulated scaling at FT. Plotting curves with equivalent electron degeneracies isolates the mixed temperature-density effect on the correlation free energy and demonstrates how the simple grouping of equivalent electron degeneracy curves is disrupted by correlation effects as the interaction approaches realistic strength.

IV. RESULTS AND DISCUSSION

The FTAC curves are observed at low, intermediate, and high temperatures and densities. In dimensionless units, typical parameters in the WDM regime are the previously introduced Wigner-Seitz radius, $r_s = r/a_B$, and the reduced temperature, $\theta = k_B\tau/E_F$, both being of order one for WDM (typically in the range of 0.1-10). Here, k_B is the Boltzmann constant, a_B is the Bohr radius, and E_F is the system's Fermi energy, defined as the zero-temperature limit of the chemical potential. By holding the density fixed as the KS system is smoothly connected to the physical system, the FTAC formalism demonstrates how the proportions of the exchange and correlation free energy components vary with temperature, density, and interaction strength. In addition, these curves invite investigation of the LO bound and its relationship to the exchange free energy.

A. Adiabatic Connection Curves

As an electronic system's temperature rises at a fixed density, it may be expected that the importance of the electron-electron interaction will decrease. However, this oversimplified picture hides the influence of both temperature and density on the components of exchange-correlation. Fig. 4 displays the adiabatic connection curves generated for a uniform gas with moderate density at temperatures varying up to the level of the Fermi energy. The solid curves of the top figure demonstrate the correlation energy while the dashed line corresponds to the exchange component of the highest-temperature curve. For clarity, the exchange component is only explicitly shown for the high-temperature curve, though similar exchange curves could be drawn, starting at $\lambda = 0$ for the exchange energy per particle for $\tau = 0.1$ and $\tau = 0.5$.

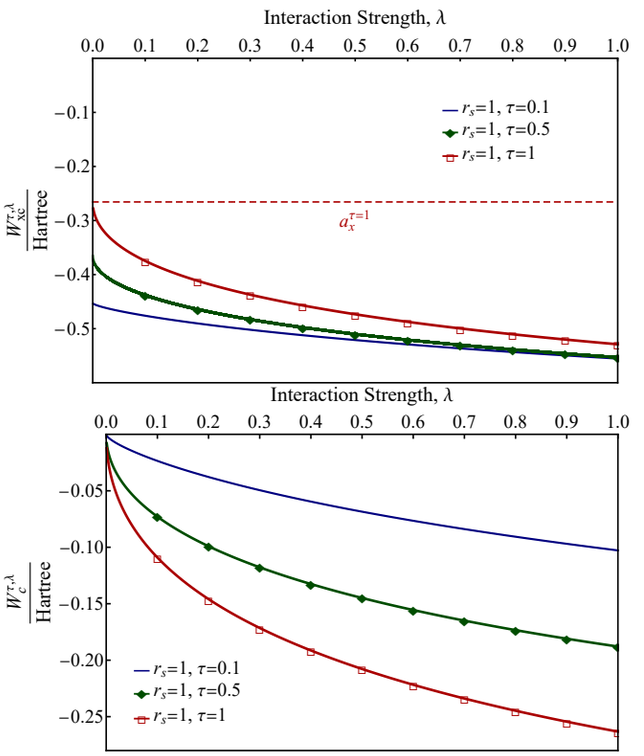

FIG. 4. FTAC curves for the UEG at a range of temperatures (top). The exchange (dashed line) is shown for the high-temperature system only. Purely correlation contributions are shown to exhibit opposite ordering with increasing temperature (bottom).

The ordering of these curves with rising temperature demonstrates that, at these conditions, the XC free energy does decrease. The bottom plot of Fig. 4, however, isolates the correlation component for all three temperatures. At these conditions, the relative contribution of correlation to a_{XC}^{τ} varies greatly with temperature. This is most easily observed in the reversal of the exchange and XC curves' ordering with temperature, but it can also be seen clearly in the flattening of the curves as we move to colder temperatures.

The curves in Fig. 5 demonstrate the adiabatic connection

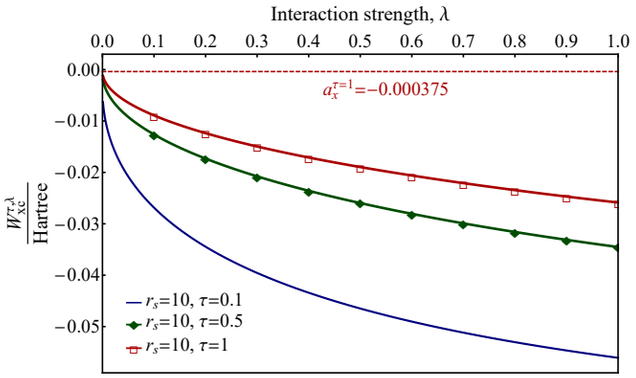

FIG. 5. FTAC curves for a low-density UEG is demonstrated for a range of temperatures. The exchange is shown only for the highest temperature. At this high r_s value, correlation clearly dominates the XC.

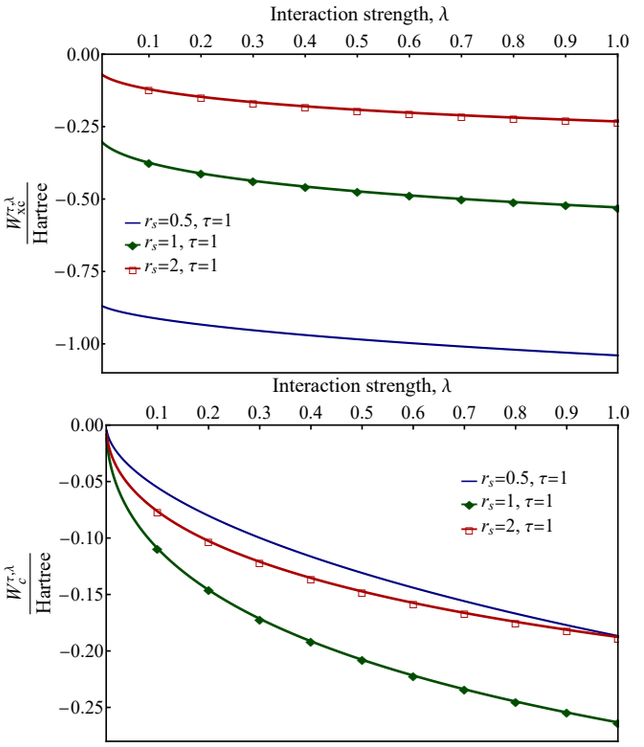

FIG. 6. FTAC curves for three different densities at a fixed temperature of $\tau = 1$ (top). Purely correlation contributions demonstrate how the ordering of the curves becomes non-monotonic when density is varied at a fixed temperature (bottom).

for a uniform gas with a relatively large Wigner-Seitz radius at low, intermediate, and high temperatures. Again, the exchange free energy component is only explicitly shown for the high-temperature curve. Since the Wigner-Seitz radius is inversely proportional to the density, a large Wigner-Seitz radius corresponds to a small density. As expected, the low-temperature curve, which was nearly linear in Fig. 4, now exhibits a fairly dramatic curvature at low λ values under these conditions. It, and all other calculated curves, obey the exact constraint of a negative first derivative.[42,66]

In contrast to the previous figures, Fig. 6 shows FTAC curves at a fixed temperature while the density is varied. Here, the XC curves show similar curvature at all densities when at the Fermi temperature, and the magnitude of the XC free energy per particle increases with increasing density. This behavior is expected since the magnitude of the exchange energy is inversely related to the Wigner-Seitz radius. The bottom plot of Fig. 6 shows the correlation contribution of each curve and demonstrates that the behavior of a_{XC}^{τ} is dominated by the exchange. Without the exchange component, the ordering of the curves is disrupted at this temperature, and we do not observe the same trend. However, at a high enough temperature, the magnitude of the correlation free energy consistently decreases with increasing r_s, or decreasing density. The differences in behavior of the correlation free energy at different temperatures demonstrate that the correlation contribution to the XC free energy fluctuates non-monotonically, as predicted via the asymmetric Hubbard dimer.[41]

B. Exact Conditions

Electron degeneracy, as defined in Eqn. 19, can be related to the Lieb-Oxford bound,[44,67] commonly expressed as an exact inequality for the potential energy contribution to the XC functional.[59] In other words, for wavefunctions that are ground states of an N-electron Hamiltonian, the adiabatic connection integrand, $W_{\mathrm{XC}}^{\lambda}$, is limited by the LO bound, where C_{LO} is the lowest possible number that makes this inequality true for all wavefunctions.[50] The LO inequality provides a strict bound on how negative the XC energy can become:

$$W_{\mathrm{XC}}^{\lambda} \geq -C_{\mathrm{LO}} \int d^3r\, n^{4/3}(\mathbf{r}), \tag{21}$$

where C_{LO} is a constant. This is often rewritten in terms of the local density approximation (LDA) to the exchange energy,

$$W_{\mathrm{XC}}^{\lambda} \geq \frac{-C_{\mathrm{LO}}}{-C_{\mathrm{X}}^{\mathrm{LDA}}} E_{\mathrm{X}}^{\mathrm{LDA}}, \tag{22}$$

where $C_{\mathrm{X}}^{\mathrm{LDA}}$ is the usual constant for the LDA exchange expression. Lieb and Oxford originally established that $C_{\mathrm{LO}} \leq 1.68$, but these bounds have since been tightened by others[46,51] to $1.444 \leq C_{\mathrm{LO}} \leq 1.636$.

Ref. 45 states that the original LO proof holds for density matrices, not only for pure states. Some preliminary evidence, based on definitions of the Hartree-exchange energy and low-density limits of A_{XC}, indicates that, though the ZT LO bound should still hold for the FTAC, bounds similar to the LO bound may be temperature-dependent in thermal DFT. In Fig. 7, FTAC curves for a fixed density are shown while the temperature is varied, along with the LO bound and a naive approach to including what might be called implicit temperature dependence. This "quick and dirty" second approach is

built on the zero-temperature expression for the LO bound for the uniform gas,

$$W_{\mathrm{XC}}^{\lambda}(r_s) \geq \frac{-C_{\mathrm{LO}}}{-C_{\mathrm{X}}^{\mathrm{LDA}}}\varepsilon_{\mathrm{X}}(r_s), \tag{23}$$

but uses the exchange-correlation free energy per particle of our system, $a_{\mathrm{X}}^{\tau}(r_s)$, in place of the zero-temperature $\varepsilon_{\mathrm{X}}(r_s)$:

$$W_{\mathrm{XC}}^{\tau,\lambda}(r_s) \geq \frac{-C_{\mathrm{LO}}}{-C_{\mathrm{X}}^{\mathrm{LDA}}}a_{\mathrm{X}}^{\tau}(r_s). \tag{24}$$

This approach would reduce the magnitude of the integral of Eqn. 21 as temperatures increase for non-uniform systems. At higher densities for the uniform gas, the FTAC curves appear to satisfy this inequality at lower temperatures. However, at a low enough density, $W_{\mathrm{XC}}^{\tau,\lambda}$ is not bound by this attempt to temperature-adjust the LO inequality, even at low temperatures. As shown in Fig. 7, only the true, zero-temperature LO bound is satisfied, whether using the 1999 value for the C_{LO} constant or the more recently tightened 2019 value. This suggests that, while LO-type bounds may exhibit some temperature dependence, it is not appropriately captured by the implicit temperature dependence of the thermally weighted density combined with the electron-degeneracy dependence of the thermal reduction factor.[24,26] In addition, the adherence of the FTAC curves to the tighter LO bound for these high-r_s (i.e., low-density) conditions indicate the density-dominated behavior of the low-temperature, low-density limit. Observing this predominately at low densities is related to the well-known dominance of correlation over exchange that holds in finite-temperature systems as well.[25] Since the exchange comprises a much smaller fraction of the total XC free energy, the correlation is large enough in relative magnitude that it dips well below the exchange-based dotted curves. As temperatures increase and the curves approach the λ-axis, it seems likely that inclusion of temperature dependence in the bound could provide a tighter bound than the ZT value, as well as for the full range of r_s and θ.

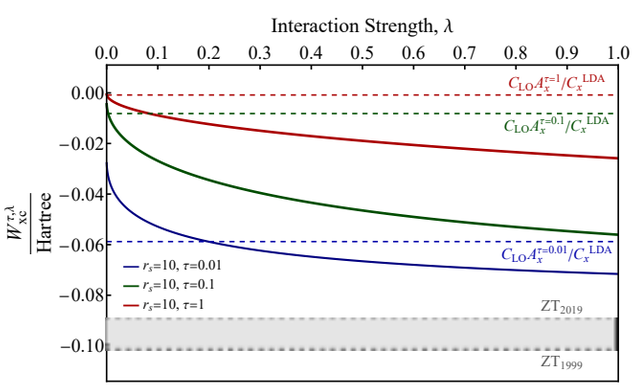

FIG. 7. ZT LO bound and temperature-adjusted quantities for a low density UEG at three different temperatures. Even at low temperatures, the XC free energy is not bounded by the LO-like line calculated from FT exchange. The shaded region indicates the range of possible values of C_{LO} in the Lieb-Oxford inequality.

One approach to investigating the temperature-dependence of the LO bound is to look at situations where the LO bound is most likely to hold; for example, when $|a_{\mathrm{X}}^{\tau}| \ll |\varepsilon_{\mathrm{X}}^{\mathrm{unif}}|$. The exchange free energy is most likely to be smaller than the ground state exchange at large values of θ. Since $\theta \propto \tau r_s^2$, a large value of theta can be achieved with a high value of τ and low value of r_s, in which the exchange component of the XC free energy dominates. A large θ may also be achieved with a low value of τ and a high value of r_s, in which the correlation component dominates.

The parameterization provided by Groth and collaborators is valid within $0 \leq \theta \leq 8$ and $0.1 \leq r_s \leq 20$. Within this range of θ values provided by Groth and coworkers,[57] $W_{\mathrm{XC}}^{\tau,\lambda=0}$ can be as small in magnitude as -0.00092 when $r_s = 20$ and $\tau \approx 0.1$, and $W^{\tau,\lambda=1}$ can be as low as -4.7780 when $r_s = 0.1$ and $\tau = 0$. Writing the inequality in terms of the uniform gas exchange per particle,[50]

$$W_{\mathrm{XC}}^{\tau,\lambda}(r_s) \geq \frac{C_{r_s,\lambda}}{C_{\mathrm{X}}^{\mathrm{LDA}}}\varepsilon_{\mathrm{X}}^{\mathrm{unif}}(r_s), \tag{25}$$

we define two approximate bounding parameters for our finite-temperature curves, $C_{\mathrm{top}} = C_{r_s,\lambda=0}$ and $C_{\mathrm{bottom}} = C_{r_s,\lambda=1}$. The r_s dependence of these two parameters is rooted in the exchange free energy's dependence on the electron degeneracy, θ, through the reduction factor. This means that maximal and minimal values are constant with respect to θ, but the value shifts depending on how one constructs this degeneracy for a given selection of r_s and its corresponding τ at that specific value of θ.

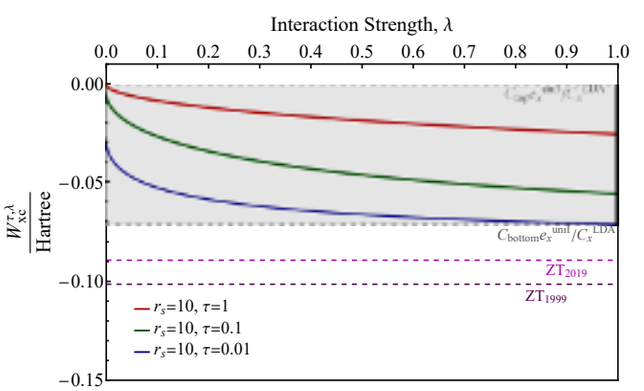

FIG. 8. Bounds are shown for FTAC curves at $r_s = 10$ and three different temperatures. The Lieb-Oxford bound, which constrains the exchange-correlation energy at ZT, is also shown for the $r_s = 10$ case.

Fig. 8 shows approximated upper and lower bounds for the FTAC for a system of $r_s = 10$ at three different temperatures. For context, the Lieb-Oxford bound for the ground-state XC energy is also shown, using both the 1999 and 2019 values for C_{LO}. As expected, the ZT bounds are more negative than either of the FT approximated constraints.

Fig. 9 shows approximated upper and lower bounds for the FTAC formalism within the allowable range of conditions for the parameterized curves. The curves correspond, from

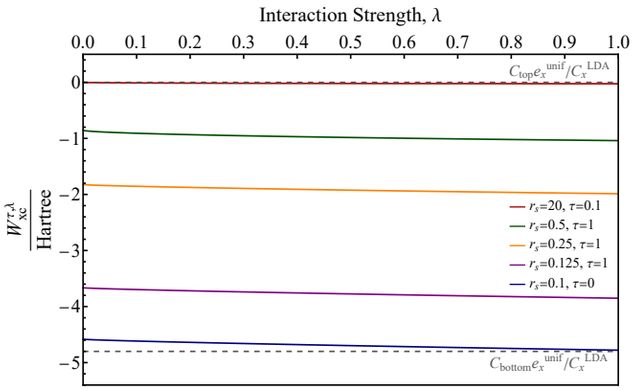

FIG. 9. Approximate upper and lower bounds generated for the FTAC formalism within the constraints of the parameterization provided by Groth and collaborators are shown for a low electron degeneracy (bottom curve), three intermediate electron degeneracy values, and a large electron degeneracy (top curve).

top to bottom, to $\theta = 8$, three intermediate electron degeneracies, and $\theta = 0$. The curve reaching the highest magnitude corresponds to $\theta = 0$, which agrees with the relationship between the exchange free energy and the thermal reduction factor, $R_X(\theta)$. This relationship, along with the dependence of the thermal reduction factor on θ, predicts that the exchange free energy decreases with increasing θ. Thus, when the electron degeneracy is low, the exchange free energy is expected to have a large magnitude, relative to exchange free energy at a high electron degeneracy.

V. SUMMARY AND FUTURE WORK

We have presented finite-temperature adiabatic connection curves based on an accurate parameterization of the exchange-correlation free energy per particle for the uniform electron gas at warm dense matter conditions.[57] Free energies obtained from the simulated scaling process[60,63,64] reproduce the directly calculated results[57] with controllable accuracy. This demonstrates the usefulness of simulated scaling for a wide range of temperatures and densities and also the reliability of the parameterization in applications beyond those for which it was originally designed.

The temperature- and density-dependent AC curves presented in this work behave as expected, in line with the ZT curve for the uniform gas in many ways. However, the relationship between density, interaction strength, and temperature is complex and combinations of conditions exist that can disrupt the naive ordering of curves based on temperature alone. As is well understood in the community, this is due to the dependence of the adiabatic connection integrand on the electron correlation. This is similar to previous calculations using the asymmetric Hubbard dimer[30,41] and supports careful use of this model system for DFT analysis. In general, the complicated behavior of the correlation free energy with temperature can be hidden by the exchange free energy, due to its strong, monotonic dependence on the electron degeneracy parameter. For careful examination of the correlation, we have demonstrated that scaling to a correlation-dominated limit can expose these details.

All curves obey the ZT Lieb-Oxford bound, as expected. However, the FT exchange free energy for the UEG does not satisfy the same relationship to this bound that the ZT exchange does, particularly in regimes of large electron degeneracy. Even at low temperatures, in low-density regimes, scaling the FT exchange free energy using the ZT Lieb-Oxford constant fails to contain the FTAC curves. In other regimes, where the magnitude of correlation is small, the exchange's dependence on temperature is strong enough to disrupt this ZT relationship. Some approximate bounds on the FTAC formalism have been generated, demonstrating the tied density-temperature effects on exchange-correlation and showing a large discrepancy between the adiabatic connection curves' most negative values and the ZT LO bound, in line with ZT analysis of similar issues. It has been shown[50] that uniform densities are not the most challenging for the LO bound at ZT, so using thermal densities near or approaching the strong-interaction limit would be a reasonable approach for better estimating any temperature dependence to be found for the LO bound.

The investigations within this work have all been undertaken within the allowed range of applicability given by Groth and coworkers, save for the initial extraction of the exchange free energy by taking a high-density (i.e., low-r_s) limit. Though this represents a deviation from the recommended usage of the parameterization, our tests using known behavior of the exchange for the UEG with the electron degeneracy demonstrate the robustness to extension beyond the low-r_s regime into the "very low" regime. Our group continues work to extend our studies of the interplay between temperature, density, and interaction strength via new approaches approximating these curves and investigating the connections between zero-temperature and finite-temperature exchange-correlation approximations. Though these methods do not rely on constraints such as the Lieb-Oxford bound, work examining the effect of temperature on bounding relationships is ongoing in hopes that connections between the two areas of study will provide insights into both the entropic contributions to the exchange-correlation free energy and the exchange-correlation as a whole.

The authors have no conflicts of interest to disclose.

VI. ACKNOWLEDGMENTS

We are grateful for useful discussions with Drs. Juri Grossi, Sara Giarrusso, and Arnold Kim. This work is supported by the U.S. Department of Energy, National Nuclear Security Administration, Minority Serving Institution Partnership Program, under Award DE-NA0003866. We acknowledge all indigenous peoples local to the site of University of California, Merced, including the Yokuts and Miwuk. We embrace their continued connection to this region and thank them for allowing us to live, work, learn, and collaborate on their tradi-

tional homeland.

REFERENCES

[1] Frank Graziani, Michael P. Desjarlais, Ronald Redmer, and Samuel B. Trickey, editors. *Frontiers and Challenges in Warm Dense Matter*, volume 96 of *Lecture Notes in Computational Science and Engineering*. Springer International Publishing, 2014.

[2] Simon Groth, Tobias Dornheim, and Michael Bonitz. Free energy of the uniform electron gas: Testing analytical models against first-principles results. *Contrib. Plasma Phys.*, 57(3):137–146, Mar 2017.

[3] M. D. Knudson and M. P. Desjarlais. Shock compression of quartz to 1.6 TPa: Redefining a pressure standard. *Phys. Rev. Lett.*, 103:225501, Nov 2009.

[4] André Kietzmann, Ronald Redmer, Michael P. Desjarlais, and Thomas R. Mattsson. Complex behavior of fluid lithium under extreme conditions. *Phys. Rev. Lett.*, 101:070401, Aug 2008.

[5] Seth Root, Rudolph J. Magyar, John H. Carpenter, David L. Hanson, and Thomas R. Mattsson. Shock compression of a fifth period element: Liquid xenon to 840 GPa. *Phys. Rev. Lett.*, 105(8):085501, Aug 2010.

[6] M. D. Knudson, M. P. Desjarlais, R. W. Lemke, T. R. Mattsson, M. French, N. Nettelmann, and R. Redmer. Probing the interiors of the ice giants: Shock compression of water to 700 gpa and 3.8 $\mathbf{g}/\mathrm{cm}^3$. *Phys. Rev. Lett.*, 108:091102, Feb 2012.

[7] B. Militzer, W. B. Hubbard, J. Vorberger, I. Tamblyn, and S. A. Bonev. A Massive Core in Jupiter Predicted from First-Principles Simulations. *Astrophys. J. Lett.*, 688(1):L45–L48, Oct 2008.

[8] Ralph Ernstorfer, Maher Harb, Christoph T. Hebeisen, Germán Sciaini, Thibault Dartigalongue, and R. J. Dwayne Miller. The Formation of Warm Dense Matter: Experimental Evidence for Electronic Bond Hardening in Gold. *Science*, 323(5917):1033–1037, Feb 2009.

[9] R. Nora, W. Theobald, R. Betti, F. J. Marshall, D. T. Michel, W. Seka, B. Yaakobi, M. Lafon, C. Stoeckl, J. Delettrez, A. A. Solodov, A. Casner, C. Reverdin, X. Ribeyre, A. Vallet, J. Peebles, F. N. Beg, and M. S. Wei. Gigabar Spherical Shock Generation on the OMEGA Laser. *Phys. Rev. Lett.*, 114(4):045001, Jan 2015.

[10] O. A. Hurricane, D. A. Callahan, D. T. Casey, E. L. Dewald, T. R. Dittrich, T. Döppner, S. Haan, D. E. Hinkel, L. F. Berzak Hopkins, O. Jones, A. L. Kritcher, S. Le Pape, T. Ma, A. G. MacPhee, J. L. Milovich, J. Moody, A. Pak, H.-S. Park, P. K. Patel, J. E. Ralph, H. F. Robey, J. S. Ross, J. D. Salmonson, B. K. Spears, P. T. Springer, R. Tommasini, F. Albert, L. R. Benedetti, R. Bionta, E. Bond, D. K. Bradley, J. Caggiano, P. M. Celliers, C. Cerjan, J. A. Church, R. Dylla-Spears, D. Edgell, M. J. Edwards, D. Fittinghoff, M. A. Barrios Garcia, A. Hamza, R. Hatarik, H. Herrmann, M. Hohenberger, D. Hoover, J. L. Kline, G. Kyrala, B. Kozioziemski, G. Grim, J. E. Field, J. Frenje, N. Izumi, M. Gatu Johnson, S. F. Khan, J. Knauer, T. Kohut, O. Landen, F. Merrill, P. Michel, A. Moore, S. R. Nagel, A. Nikroo, T. Parham, R. R. Rygg, D. Sayre, M. Schneider, D. Shaughnessy, D. Strozzi, R. P. J. Town, D. Turnbull, P. Volegov, A. Wan, K. Widmann, C. Wilde, and C. Yeamans. Inertially confined fusion plasmas dominated by alpha-particle self-heating. *Nat. Phys.*, 12(8):800–806, Apr 2016.

[11] P. Hohenberg and W. Kohn. Inhomogeneous electron gas. *Phys. Rev.*, 136(3B):B864–B871, Nov 1964.

[12] W. Kohn and L. J. Sham. Self-consistent equations including exchange and correlation effects. *Phys. Rev.*, 140(4A):A1133–A1138, Nov 1965.

[13] Thomas R. Mattsson and Michael P. Desjarlais. Phase diagram and electrical conductivity of high energy-density water from density functional theory. *Phys. Rev. Lett.*, 97:017801, Jul 2006.

[14] Winfried Lorenzen, Bastian Holst, and Ronald Redmer. Demixing of hydrogen and helium at megabar pressures. *Phys. Rev. Lett.*, 102:115701, Mar 2009.

[15] M. D. Knudson, M. P. Desjarlais, A. Becker, R. W. Lemke, K. R. Cochrane, M. E. Savage, D. E. Bliss, T. R. Mattsson, and R. Redmer. Direct observation of an abrupt insulator-to-metal transition in dense liquid deuterium. *Science*, 348(6242):1455–1460, Jun 2015.

[16] Bastian Holst, Ronald Redmer, and Michael P. Desjarlais. Thermophysical properties of warm dense hydrogen using quantum molecular dynamics simulations. *Phys. Rev. B*, 77:184201, May 2008.

[17] M. D. Knudson, M. P. Desjarlais, and Aurora Pribram-Jones. Adiabatic release measurements in aluminum between 400 and 1200 GPa: Characterization of aluminum as a shock standard in the multimegabar regime. *Phys. Rev. B*, 91(22):224105, Jun 2015.

[18] R F Smith, J H Eggert, R Jeanloz, T S Duffy, D G Braun, J R Patterson, R E Rudd, J Biener, A E Lazicki, A V Hamza, J Wang, T Braun, L X Benedict, P M Celliers, and G W Collins. Ramp compression of diamond to five terapascals. *Nature*, 511(7509):330–3, Jul 2014.

[19] Zhandos Moldabekov, Tobias Dornheim, Maximilian Böhme, Jan Vorberger, and Attila Cangi. The relevance of electronic perturbations in the warm dense electron gas. *J. Chem. Phys.*, 155(12):124116, Sep 2021.

[20] Tobias Dornheim, Maximilian Böhme, Zhandos A. Moldabekov, Jan Vorberger, and Michael Bonitz. Density Response of the Warm Dense Electron Gas beyond Linear Response Theory: Excitation of Harmonics. *arXiv*, Apr 2021.

[21] Zhandos Moldabekov, Tobias Dornheim, Jan Vorberger, and Attila Cangi. Benchmarking Exchange-Correlation Functionals in the Spin-Polarized Inhomogeneous Electron Gas under Warm Dense Conditions. *arXiv*, Oct 2021.

[22] N. D. Mermin. Thermal properties of the inhomogenous electron gas. *Phys. Rev.*, 137:A: 1441, 1965.

[23] M. W. C. Dharma-wardana and R. Taylor. Exchange and correlation potentials for finite temperature quantum calculations at intermediate degeneracies. *J. Phys. C: Solid State Phys.*, 14(5):629–646, Feb 1981.

[24] François Perrot and M. W. C. Dharma-wardana. Exchange and correlation potentials for electron-ion systems at finite temperatures. *Phys. Rev. A*, 30(5):2619–2626, Nov 1984.

[25] S. Pittalis, C. R. Proetto, A. Floris, A. Sanna, C. Bersier, K. Burke, and E. K. U. Gross. Exact conditions in finite-temperature density-functional theory. *Phys. Rev. Lett.*, 107:163001, Oct 2011.

[26] Aurora Pribram-Jones, Stefano Pittalis, E.K.U. Gross, and Kieron Burke. Thermal density functional theory in context. In Frank Graziani, Michael P. Desjarlais, Ronald Redmer, and Samuel B. Trickey, editors, *Frontiers and Challenges in Warm Dense Matter*, volume 96 of *Lecture Notes in Computational Science and Engineering*, pages 25–60. Springer International Publishing, 2014.

[27] Valentin V. Karasiev, Travis Sjostrom, and S. B. Trickey. Generalized-gradient-approximation noninteracting free-energy functionals for orbital-free density functional calculations. *Phys. Rev. B*, 86:115101, Sep 2012.

[28] Attila Cangi and Aurora Pribram-Jones. Efficient formalism for warm dense matter simulations. *Phys. Rev. B*, 92:161113, Oct 2015.

[29] Valentin V. Karasiev, Lázaro Calderín, and S. B. Trickey. Importance of finite-temperature exchange correlation for warm dense matter calculations. *Phys. Rev. E*, 93(6):063207, Jun 2016.

[30] J. C. Smith, A. Pribram-Jones, and K. Burke. Exact thermal density functional theory for a model system: Correlation components and accuracy of the zero-temperature exchange-correlation approximation. *Phys. Rev. B*, 93(24):245131, Jun 2016.

[31] Valentin V. Karasiev, S. B. Trickey, and James W. Dufty. Status of free-energy representations for the homogeneous electron gas. *Phys. Rev. B*, 99(19):195134, May 2019.

[32] V. V. Karasiev, S. X. Hu, M. Zaghoo, and T. R. Boehly. Exchange-correlation thermal effects in shocked deuterium: Softening the principal Hugoniot and thermophysical properties. *Phys. Rev. B*, 99(21):214110, Jun 2019.

[33] Tobias Dornheim, Jan Vorberger, and Michael Bonitz. Nonlinear electronic density response in warm dense matter. *Phys. Rev. Lett.*, 125:085001, Aug 2020.

[34] Kushal Ramakrishna, Tobias Dornheim, and Jan Vorberger. Influence of finite temperature exchange-correlation effects in hydrogen. *Phys. Rev. B*, 101(19):195129, May 2020.

[35] Francisca Sagredo and Kieron Burke. Confirmation of the pplb derivative discontinuity: Exact chemical potential at finite temperatures of a model system. *Journal of Chemical Theory and Computation*, 16(12):7225–7231, 2020. PMID: 33237784.

[36] D. I. Mihaylov, V. V. Karasiev, S. X. Hu, J. R. Rygg, V. N. Goncharov, and G. W. Collins. Improved first-principles equation-of-state table of deu-

terium for high-energy-density applications. *Phys. Rev. B*, 104(14):144104, Oct 2021.
[37]Zhandos Moldabekov, Tobias Dornheim, Maximilian Böhme, Jan Vorberger, and Attila Cangi. The relevance of electronic perturbations in the warm dense electron gas. *The Journal of Chemical Physics*, 155(12):124116, 2021.
[38]J. Harris and A. Griffin. *Phys. Rev. B*, 11:3669, 1975.
[39]D.C. Langreth and J.P. Perdew. The exchange-correlation energy of a metallic surface. *Solid State Commun.*, 17:1425, 1975.
[40]O. Gunnarsson and B.I. Lundqvist. Exchange and correlation in atoms, molecules, and solids by the spin-density-functional formalism. *Phys. Rev. B*, 13:4274, 1976.
[41]Justin C. Smith, Francisca Sagredo, and Kieron Burke. *Warming Up Density Functional Theory*. Springer, Singapore, Nov 2017.
[42]M. Levy and J.P. Perdew. Hellmann-Feynman, virial, and scaling requisites for the exact universal density functionals. shape of the correlation potential and diamagnetic susceptibility for atoms. *Phys. Rev. A*, 32:2010, 1985.
[43]M. Levy. Density-functional exchange-correlation through coordinate scaling in adiabatic connection and correlation hole. *Phys. Rev. A*, 43:4637, 1991.
[44]Mel Levy. Universal variational functionals of electron densities, first-order density matrices, and natural spin-orbitals and solution of the *v*-representability problem. *Proceedings of the National Academy of Sciences of the United States of America*, 76(12):6062–6065, 1979.
[45]Elliott H. Lieb and Stephen Oxford. Improved lower bound on the indirect coulomb energy. *International Journal of Quantum Chemistry*, 19(3):427–439, 1981.
[46]Garnet Kin-Lic Chan and Nicholas C. Handy. Optimized lieb-oxford bound for the exchange-correlation energy. *Phys. Rev. A*, 59:3075–3077, Apr 1999.
[47]Mariana M. Odashima and K. Capelle. How tight is the Lieb-Oxford bound? *arXiv*, Apr 2007.
[48]Mariana M. Odashima, K. Capelle, and S. B. Trickey. Tightened Lieb-Oxford Bound for Systems of Fixed Particle Number. *J. Chem. Theory Comput.*, 5(4):798–807, Apr 2009.
[49]Mathieu Lewin and Elliott H. Lieb. Improved lieb-oxford exchange-correlation inequality with a gradient correction. *Phys. Rev. A*, 91:022507, Feb 2015.
[50]Michael Seidl, Stefan Vuckovic, and Paola Gori-Giorgi. Challenging the Lieb–Oxford bound in a systematic way. *Mol. Phys.*, 114(7-8):1076–1085, Apr 2015.
[51]Mathieu Lewin, Elliott H. Lieb, and Robert Seiringer. Floating wigner crystal with no boundary charge fluctuations. *Phys. Rev. B*, 100:035127, Jul 2019.
[52]J.P. Perdew. *Physica B*, 172:1, 1991.
[53]John P. Perdew, Kieron Burke, and Matthias Ernzerhof. Generalized gradient approximation made simple. *Phys. Rev. Lett.*, 77(18):3865–3868, Oct 1996. *ibid.* **78**, 1396(E) (1997).
[54]John P. Perdew, Adrienn Ruzsinszky, Jianwei Sun, and Kieron Burke. Gedanken densities and exact constraints in density functional theory. *The Journal of Chemical Physics*, 140(18):–, 2014.
[55]Jianwei Sun, John P. Perdew, and Adrienn Ruzsinszky. Semilocal density functional obeying a strongly tightened bound for exchange. *Proc. Natl. Acad. Sci. U.S.A.*, 112(3):685–689, Jan 2015.
[56]Valentin V. Karasiev, James W. Dufty, and S.B. Trickey. Nonempirical semilocal free-energy density functional for matter under extreme conditions. *Phys. Rev. Lett.*, 120:076401, Feb 2018.
[57]Simon Groth, Tobias Dornheim, Travis Sjostrom, Fionn D. Malone, W. M. C. Foulkes, and Michael Bonitz. Ab initio exchange-correlation free energy of the uniform electron gas at warm dense matter conditions. *Phys. Rev. Lett.*, 119:135001, Sep 2017.
[58]A. L. Fetter and J. D. Walecka. *Quantum theory of many-particle systems*. McGraw-Hill, New York, NY, 1971.
[59]Kieron Burke and friends. The ABC of DFT. In preparation.
[60]A. Pribram-Jones and K. Burke. Connection formulas for thermal density functional theory. *Phys. Rev. B*, 93:205140, May 2016.
[61]M. Levy. *Int. J. Quantum Chem.*, S23:617, 1989.
[62]Y. Wang and J. P. Perdew. *Phys. Rev. B*, 43:8911, 1991.
[63]W. Terilla D. Frydel and K. Burke. Adiabatic connection from accurate wavefunction calculations. *J. Chem. Phys.*, 112:5292, 2000.
[64]W. Terilla R.J. Magyar and K. Burke. Accurate adiabatic connection curve beyond the physical interaction strength. *J. Chem. Phys.*, 119:696, 2003.
[65]Wolfram Research, Inc. Mathematica, Version 11.2. Champaign, IL, 2020.
[66]A. M. Teale, S. Coriani, and T. Helgaker. Accurate calculation and modeling of the adiabatic connection in density functional theory. *The Journal of Chemical Physics*, 132(16):164115, 2010.
[67]Elliott H. Lieb and Stephen Oxford. Improved lower bound on the indirect Coulomb energy. *Int. J. Quantum Chem.*, 19(3):427–439, Mar 1981.

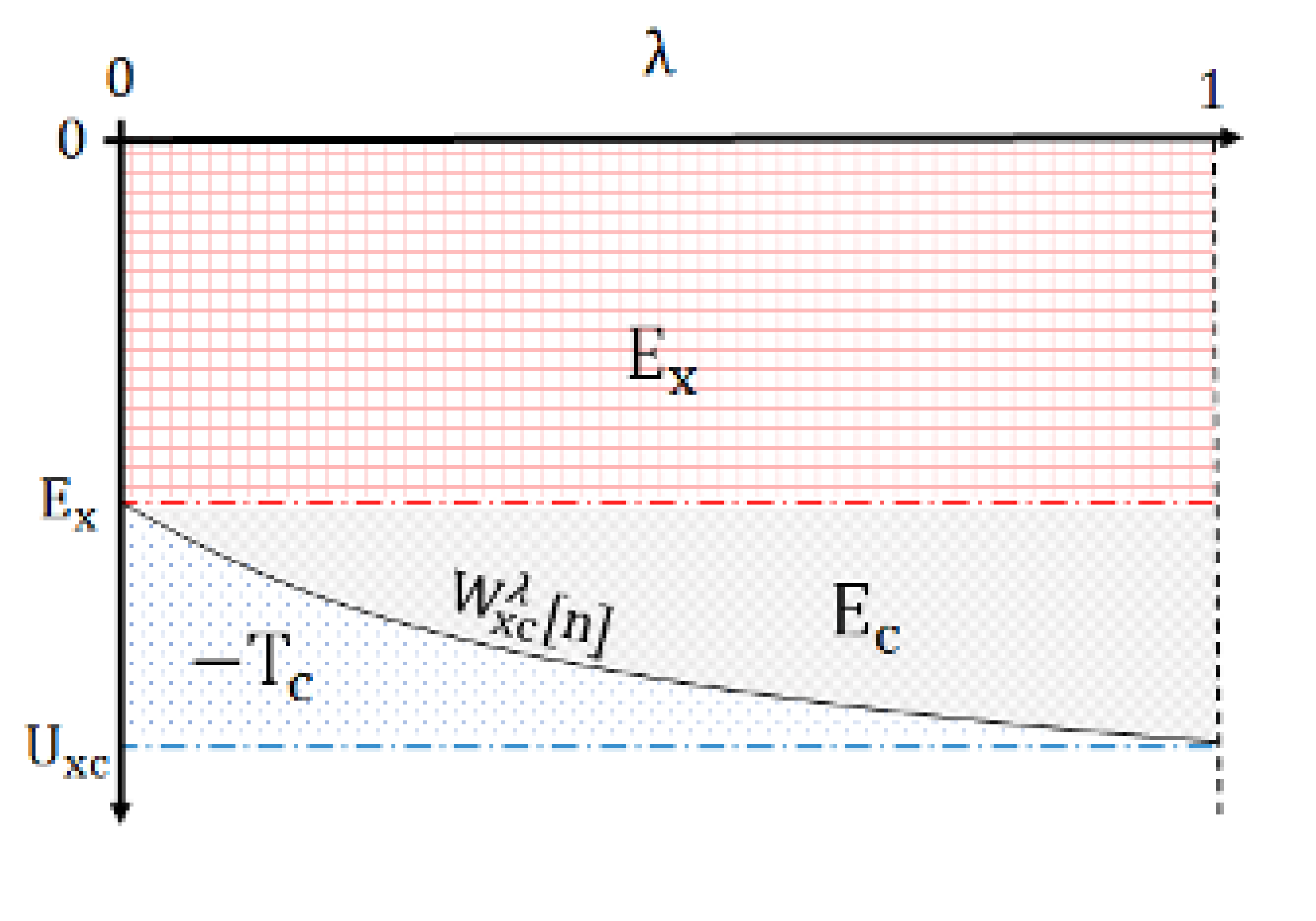
λ
0
1
0
E_x
E_x
$W_{xc}^{\lambda}[n]$
E_c
$-T_c$
U_{xc}

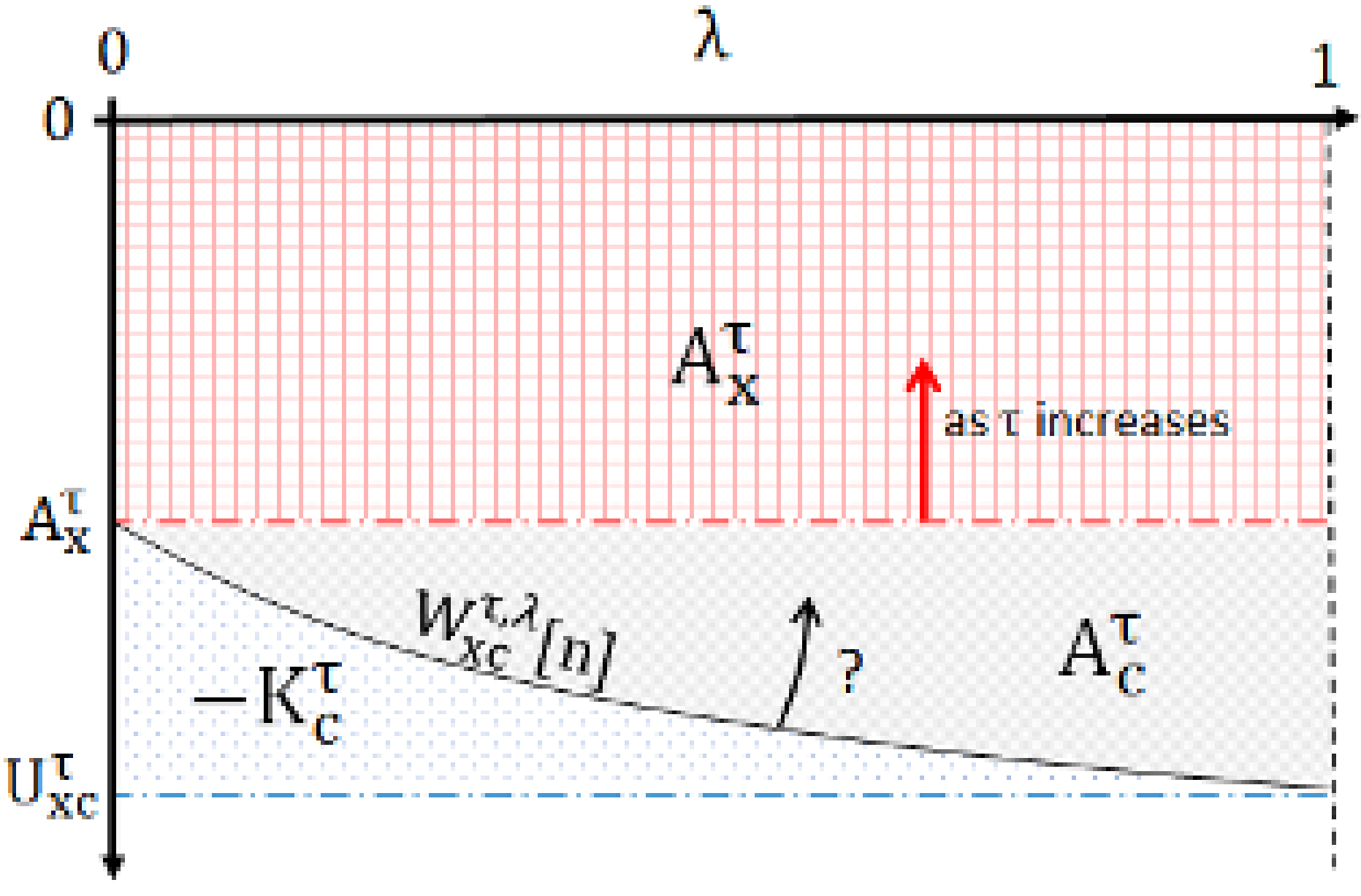
0
λ
1
0
A_x^τ
as τ increases
A_x^τ
$W_{xc}^{\tau,\lambda}[n]$
?
A_c^τ
$-K_c^\tau$
U_{xc}^τ